

Gravitational lensing of type Ia supernovae by galaxy clusters

Tsafrir S. Kolatt¹

The Physics Department and Lick Observatory, University of California, Santa Cruz, CA 95064,
U.S.A.

and

Matthias Bartelmann²

Max-Planck-Institut für Astrophysik, P.O. Box 1523, D-85740 Garching, Germany

ABSTRACT

We propose a method to remove the mass sheet degeneracy that arises when the mass of galaxy clusters is inferred from gravitational shear. The method utilizes high-redshift standard candles that undergo weak lensing. Natural candidates for such standard candles are type Ia supernovae (SN Ia).

When corrected with the light-curve shape (LCS), the peak magnitude of SN Ia provides a standard candle with an uncertainty in apparent magnitude of $\Delta m \simeq 0.1 - 0.2$. Gravitational magnification of a background SN Ia by an intervening cluster would cause a mismatch between the observed SN Ia peak magnitude compared to that expected from its LCS and redshift. The average detection rate for SN Ia with a significant mismatch of $\geq 2\Delta m$ behind a cluster at $z \simeq 0.05 - 0.15$ is about 1 – 2 supernovae per cluster per year at $J, I, R \lesssim 25 - 26$.

Since SNe are point-like sources for a limited period, they can experience significant microlensing by MACHOs in the intracluster medium. Microlensing events caused by MACHOs of $\sim 10^{-4} M_{\odot}$ are expected to have time scales similar to that of the SN light curve. Both the magnification curve by a MACHO and the light curve of a SN Ia have characteristic shapes that allow to separate them. Microlensing events due to MACHOs of smaller mass can unambiguously be identified in the SN light curve if the latter is continuously monitored. The average number of identifiable microlensing events per nearby cluster ($z \lesssim 0.05$) per year is $\sim 0.02(f/0.01)$, where f is the fraction of the cluster mass in MACHOs of masses $10^{-7} < M_{\text{macho}}/M_{\odot} < 10^{-4}$.

Subject headings: Cosmology: Gravitational Lensing – Dark Matter, Galaxies: Clusters: general, Methods: Miscellaneous

¹email:tsafir@physics.ucsc.edu

²email:mbartelmann@mpa-garching.mpg.de

1. Introduction

The mass sheet degeneracy (Falco, Gorenstein, & Shapiro 1985; Schneider & Seitz 1995) constitutes one of the fundamental uncertainties in attempts at reconstructing galaxy cluster masses from the gravitational distortion of resolved background sources. It arises because the observed gravitational shear field is insensitive to magnification. A few methods were proposed to break the degeneracy by directly measuring either the magnification or the (scaled) surface mass density. Broadhurst, Taylor, & Peacock (1995) suggested to compare the redshift and/or the magnitude distribution of the background sources in cluster fields with those measured in empty fields. Kaiser (1995) and Kneib *et al.* (1995) showed that inferring the mean source redshift at a given apparent magnitude can help to break the degeneracy. Bartelmann & Narayan (1995) proposed and tested an algorithm that exploits the size distribution of the background sources and the conservation of surface brightness under gravitational lensing. An alternative cluster reconstruction technique suggested by Bartelmann *et al.* (1996) breaks the mass sheet degeneracy by simultaneously taking sizes *and* shapes of background galaxies into account. All these methods rest upon statistical information on intrinsic background galaxy sizes. They require accurate measurements of sizes and magnitudes or surface brightnesses of lensed galaxies. In principle, a single sufficiently precise measurement of the magnification of a standard candle by a cluster can lift the mass sheet degeneracy as well.

Suppose a standard candle is observed behind a lens, and its redshift is measured. Assuming a cosmological model, the luminosity distance is known. The apparent magnitude expected from its luminosity can then be compared to the observed one, and any discrepancy between the two can be attributed to the magnification by the foreground lens. Ideal standard candles are rare in cosmology. Nevertheless, there is accumulating strong evidence that SN Ia may well serve as approximate standard candles, especially if one takes the dependence of their peak magnitude on the light curve shape into account (Phillips 1993; Riess, Press, & Kirshner 1995 (RPK1); Riess, Press, & Kirshner 1996 (RPK2); Hamuy *et al.* 1996a). Moreover, SN Ia are ubiquitous, point-like sources, their distinct spectral lines allow for an accurate redshift determination, and as of yet they show no cosmological evolution. Though rare in frequency, each of their aforementioned characteristics makes SN Ia excellent probes for the integrated matter density along their lines-of-sight, and the composition of the matter (*i.e.* its graininess, occurrence of MACHOs etc.). Weak lensing by large-scale structure was shown to not significantly affect the SN magnitude (Frieman 1996; Wambsganss *et al.* 1996), but this does not apply to galaxy clusters.

Similar arguments led Kovner & Paczyński (1988) to propose a possible identification of SNe in giant arcs as a tool to establish the time delay between different images. Giant arcs are less appealing than weak lensing by clusters because they are much more rare, and sensitive to the details of the density profile close to the cluster core.

Soucail & Fort (1991) suggested the combination of giant arcs and a much less accurate “standard candle”, viz. the Tully-Fisher relation, to estimate the Hubble constant. This method suffers

from several difficulties, *e.g.* a possible cosmological evolution of the Tully-Fisher relation, and the problematic determination of the inclination angle of the lensed galaxy.

In the rest of this paper, we present the basic considerations one has to take into account in order to employ SN Ia for these purposes. In §2 we review the necessary facts about the SN population and the cluster model we use. In §3 we estimate the number of expected SN in the background of a cluster, whose luminosity–distance mismatch is large enough to allow for the removal of the mass sheet degeneracy. In §4 we discuss the use of a lensed SN Ia as a probe for MACHOs in the intracluster medium. We conclude with our results in §5.

2. Supernovae and clusters

2.1. Supernovae Type Ia

The distribution of absolute peak magnitudes of SN Ia is intrinsically narrow (see Branch & Tammann 1992 for a review). From the Hamuy *et al.* (1996a,b) sample, we find the average absolute magnitude and its standard deviation to be $(-18.12, 0.38)$, $(-18.19, 0.26)$, $(-17.97, 0.19)$, for $\langle M_{\text{SN}} \rangle + 5 \log h$ in the B, V, and I bands, respectively³. The quoted standard deviation is larger than the intrinsic one, since Hamuy *et al.* did not correct for reddening due to dust in the host galaxies. Figure 1a shows the absolute-magnitude distribution of the sample. These results are in accord with Branch & Miller (1993) [$(-18.2 + 5 \log h, 0.36)$ in B], and Vaughan *et al.* (1995) [$(-18.28 + 5 \log h, 0.31)$ for a sub-sample]. The latter two results were obtained by cross-comparison with other distance indicators, that are only available for relatively nearby galaxies. The results may therefore suffer from the intrinsic scatter in these other distance indicators. The Hamuy *et al.* (1996a) sample includes distant galaxies (up to $z = 0.1$) whose redshift provides a good enough distance estimate.

A substantial decrease in the scatter of the peak luminosity distribution is achieved if a correction that is based on the shape of the light curve (LCS) is applied in different bands (Phillips 1993; RPK1, RPK2, Hamuy *et al.* 1996a). This can also account for reddening due to dust in the host galaxy, the Milky Way, and possibly in the foreground cluster. After the correction, SN Ia can be regarded as standard candles up to a small dispersion of $\Delta m \simeq 0.1 - 0.2$.

A parameter that is traditionally taken to govern the LCS is the decline in B magnitude 15 rest-frame days after maximum light, ΔM_{15} . According to the Hamuy *et al.* (1996a) data, its distribution has a mean and standard deviation of $(1.28, 0.28)$, respectively. Figure 1b shows the distribution of the rest-frame ΔM_{15} from the 29 Hamuy *et al.* (1996a) SNe. The small dispersion in ΔM_{15} is a reflection of similar timescales for the rise and decline of the light curves of different SN. In §3.2 we shall use a rise time of 5 rest-frame days. This corresponds to a magnitude difference of

³Hereafter, M_{SN} is the absolute blue peak magnitude.

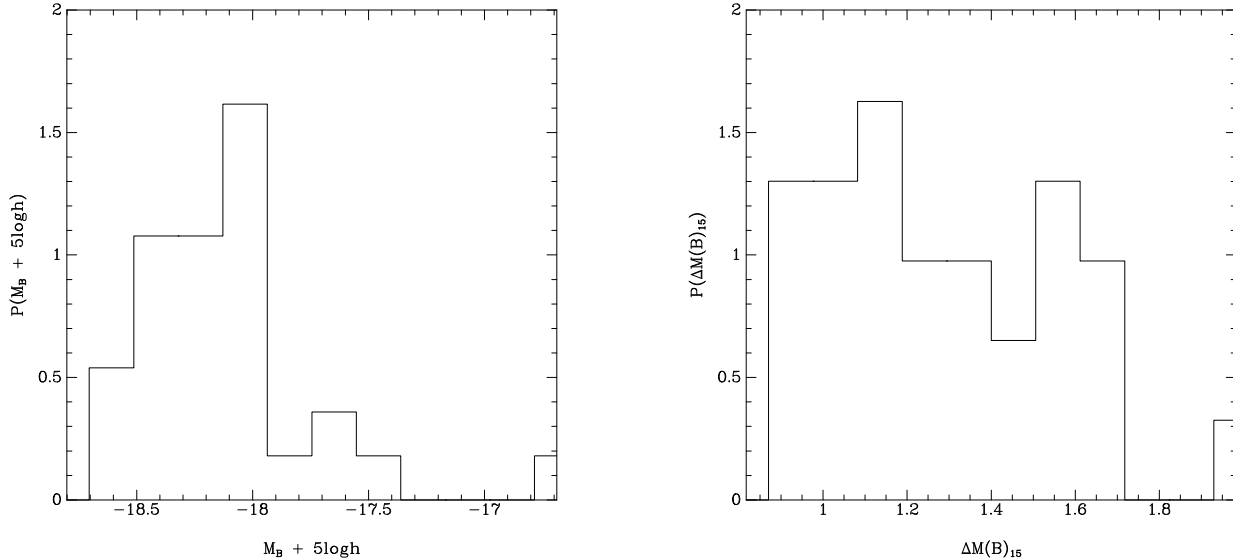


Fig. 1.— The frequency distribution of the absolute B magnitude from the Hamuy *et al.* (1996a,b) sample of 29 SNe Ia (left), and the distribution of the magnitude difference 15 (rest-frame) days past the peak for the same sample (right).

about $\Delta M_{-5} = |M_{\text{SN}} - M_{\text{SN}-5}| \sim 0.1 - 0.3$.

The specific rate of SNe Ia, \mathcal{S}_{SN} , (measured in SNU: SN per $10^{10} L_{B\odot}$ per century) shows a rise with redshift. The local specific rate, $\mathcal{S}_{\text{SN}}(z = 0)$, is estimated to lie between $0.2h^2$ and $0.7h^2$ SNU, depending on the host galaxy type (Cappellaro *et al.* 1993a, 1993b; Turatto, Cappellaro, & Benetti 1994; van den Bergh & McClure 1994; Muller *et al.* 1992). The average rate at $z = 0.4$ is estimated to be $\simeq 0.82h^2$ SNU (Pain *et al.* 1996). The rate evolution may depend on galaxy evolution, the stellar mass function, different composition of late and early type galaxies at different redshifts, and a different fraction of massive blue stars that undergo a SN Ia phase.

Even though the evidence for a rise with redshift is still inconclusive, all of these dependencies lead to an increment of the average specific rate of SN Ia with redshift. Hamuy *et al.* (1995) suggest that galaxies with younger stellar population produce the most luminous SNe. Branch, Romanishin, & Baron (1996) argue that SNe Ia preferentially reside in late type spirals. It is hence natural to expect a higher average specific rate of SN Ia at higher redshifts.

2.2. The Cluster Model

All theoretical and observationally motivated models for cluster density profiles agree on its parametric shape ($\propto r^{-2}$) at intermediate radii ($\sim 0.1 - 1.5 h^{-1}\text{Mpc}$) between its core and outskirts (*e.g.* Gunn & Gott 1972; Filmore & Goldreich 1984; Bertschinger 1985; Hoffman 1988). Mass profiles obtained from weak lensing corroborate this parametric form for a few specific cluster examples (*e.g.* Tyson & Fischer 1995). N-body simulations show a similar behavior (*e.g.* Navarro, Frenk, & White 1996). We hence use a singular isothermal sphere (SIS) as our cluster model, *i.e.* a density profile of $\rho(r) = (\sigma_v/c)^2/(2\pi G)r^{-2}$, where σ_v is the one-dimensional velocity dispersion. Cluster cores, if they exist, are of size $\lesssim 100 h^{-1}\text{kpc}$, beyond which the cluster profile resembles the SIS profile. Note that this is the scale where weak lensing starts to serve as a tool for deriving the cluster density profile, and thus where the mass-sheet degeneracy comes in. Since most SN Ia lensed by clusters are expected to be found at radii larger than the core, the approximation of a SIS profile is good enough for our purposes. At the other end, we are limited by the minimal magnification for a mismatch identification. This requirement sets the outer radius of interest. This radius is always smaller than the scale where the asymptotic behavior of the cluster density profile differs from SIS for different models.

For a SIS, the magnification of an image at angular distance θ from the cluster center is given by

$$A(\theta) = \left[1 - \frac{\theta_E}{\theta}\right]^{-1}; \quad \theta_E = \frac{D_{\text{LS}}}{D_S} 4\pi \left(\frac{\sigma_v}{c}\right)^2. \quad (2-1)$$

D_S and D_{LS} are the angular diameter distances to the source, and between the lens and the source, respectively. θ_E is the Einstein angle of the cluster. For $\theta < 2\theta_E$, two images appear on either side of the lens, the fainter one being at $\theta < \theta_E$, and the brighter one at $\theta > \theta_E$. We ignore the fainter image in the following, thus having $\theta \geq \theta_E$ and $A \geq 1$ always.

The cross section for sources that are magnified by more than $A \geq A_{\text{min}} \geq 1$ by a SIS foreground lens is

$$\sigma_{\text{SIS}}(A) = \frac{\pi\theta_E^2}{(A-1)^2}. \quad (2-2)$$

Hence, magnifications $A \geq A_{\text{min}}$ are distributed according to

$$P(A) \propto -\frac{d\sigma_{\text{SIS}}(A)}{dA}; \quad P(A)dA = \frac{2(A_{\text{min}}-1)^2}{(A-1)^3}dA, \quad (2-3)$$

where the second expression follows from the normalization $\int_{A_{\text{min}}}^{\infty} P(A)dA = 1$.

3. Estimation of the observed SN rate

We model the quality of the SN to serve as standard candles in terms of the natural width, Δm , of the LCS–magnitude–distance relation.

The magnification by a cluster boosts the apparent magnitude by $-2.5 \log_{10} A(\theta)$. If the boost is large enough, a mismatch between the SN apparent magnitude (corrected by the LCS) and its luminosity distance will show up.

The luminosity distance is calculated from the SN redshift, given the cosmological parameters (Ω_m , Ω_Λ , ($\Omega_k = 1 - \Omega_m - \Omega_\Lambda$) and H_0). The closer the SN is to the cluster center, the larger is the magnification A , and the more pronounced is the discrepancy. The boost allows to observe sources that without the presence of the lens would fall below the detection flux limit. A competing effect of the lens is the reduction of the surface number density of background sources by $A(\theta)^{-1}$.

The bigger the cluster appears on the sky, the more background galaxies it encompasses, and thus the more potential SNe. This geometrical effect must be combined with the competing D_{LS}/D_S term in the magnification (eq. 2-1).

We assume all SNe reside in galaxies. We do not distinguish between early and late type galaxies, as SN Ia occur in both, though there is an indication that SNe are more frequent in late-type galaxies (Cappellaro *et al.* 1997). The relevant function one needs to know is thus $n(z)$, the number density of galaxies at redshift z , and their luminosity distribution. It is also essential to know what the average number of SNe is for these galaxies at a given redshift. If the rest-frame blue luminosity function of galaxies at the relevant redshift is known, we may adopt a value for the specific SN rate, \mathcal{S}_{SN} , and obtain the SN Ia average rate per proper time unit per comoving volume unit from

$$\mathcal{S}_{\text{SN}}(z) = \mathcal{S}_{\text{SN}}(z) \int_{-\infty}^{\infty} dL L P(L, z), \quad (3-1)$$

with $P(L, z)$ the Schechter luminosity function at redshift z (*cf.* §3.1). For this calculation it is essential to have an estimate for $P(L, z)$, the normalization and the parameters of the Schechter function at each redshift, or its integral – the number density of galaxies at each redshift.

3.1. Galaxy number density at different redshifts

The best estimate to date for the number density of galaxies as function of redshift at $z > 0.3$ comes from the Canada-France redshift survey (CFRS). Lilly *et al.* (1995) estimated the Schechter function parameters in the rest-frame B band in three redshift bins⁴. At lower redshift, we adopt the estimates for these parameters from the APM survey (Loveday *et al.* 1992) and the AUTOFIB survey (Ellis *et al.* 1996). In order to get the overall galaxy density in a given redshift bin, we integrate the Schechter function with the adopted parameters over the range $(-\infty, M_{\text{lim}}]$. M_{lim} is the minimum absolute magnitude that prevents divergence of the integral.

Figure 2 shows the number density for five different values of M_{lim} as a function of redshift. For the CFRS, we took the parameters of their “best” estimate with $q_0 = 0.5$. The points represent

⁴We translated the CFRS B_{AB} to B to comply with the notation in the rest of this paper.

the center of the bin (not volume weighted), and the diagonal line is an approximate behavior of a linear function guided by all the surveys' points⁵.

The highest redshift bin of the CFRS ends at $z = 1$. For the current analysis we need to extrapolate $n(z)$ beyond that limit. We need to know how far one can safely extrapolate the approximation, and to what extent the functional form and the derived parameters are adequate.

A good verification for estimates of the galaxy number density as a function of redshift is the calculated surface number density of galaxies in a given apparent magnitude limit. Observed values for the surface number density range between $50 - 100 \text{ arcmin.}^{-2}$ for $B \sim 25 - 27.5$, corresponding to $R \sim 24 - 26.5$ (Tyson 1988; Lilly, Cowie, & Gardner 1991; Metcalfe *et al.* 1991, 1995), and as high as $\sim 200 \text{ arcmin.}^{-2}$ for $R \sim 27$ (Smail *et al.* 1995). If we consider all galaxies with $M < -17 + 5 \log h (= M_{\text{lim}})$, and apply an apparent magnitude limit of $m < 26$, and use the relations given in Fig. 2 ($n(z) = a + bz$), we find that integration out to $z_S \simeq 2.0$ yields surface densities of $\sim 60 - 70 \text{ arcmin.}^{-2}$. Integration out to $z = 1.5$ yields 45 arcmin.^{-2} . Note that we did not model the K-correction, and assigned only rest-frame B magnitudes to the galaxies. The limit we quote is thus roughly equivalent to an R or I magnitude limit.

Since the integration we performed over the functions shown in Fig. 2 along redshift yields a similar surface number density as observed, we may safely adopt the form $n(z) = a + bz$ as our estimate for the redshift dependence of galaxy number density. We extrapolate the functional form and parameters from the observational data to $z = 2.0$ in order to achieve the right surface number density, but we do not attempt to extrapolate any further, even though it may increase the resultant rate of SN Ia detection. The parameters (a and b of the last expression) for different cutoffs in rest-frame absolute B magnitude appear in fig. 2. Recall we need the galaxy number density only in order to know the size of the reservoir from which observable SNe are taken, and to estimate the upper limit of the redshift. The magnitude limit of the proposed SN Ia survey is irrelevant to the host galaxy luminosity.

3.2. The rate calculation

Using the same parameters for the Schechter luminosity function, we calculate the SN rate per century per unit of comoving volume, S_{SN} , at different redshifts (eq. 3-1). Figure 3 shows this rate. We choose our base-line specific rate to be $S_{\text{SN}} = 0.82h^2 \text{ SNU}$ from the $z = 0.4$ estimate (Pain *et al.* 1996). We expect most of the host galaxies to lie beyond this redshift. We ignore a possible increase of this base-line with redshift. The change of S_{SN} in fig. 3 is therefore entirely due to the change in the Schechter function parameters. We model this change crudely by a linear

⁵We did not perform a least square linear fit because Lilly *et al.* warn the reader not to take their fitting parameters beyond their fitting range, and because the errors in different surveys do not necessarily have a common reference ground. We tried to always *underestimate* the function slope.

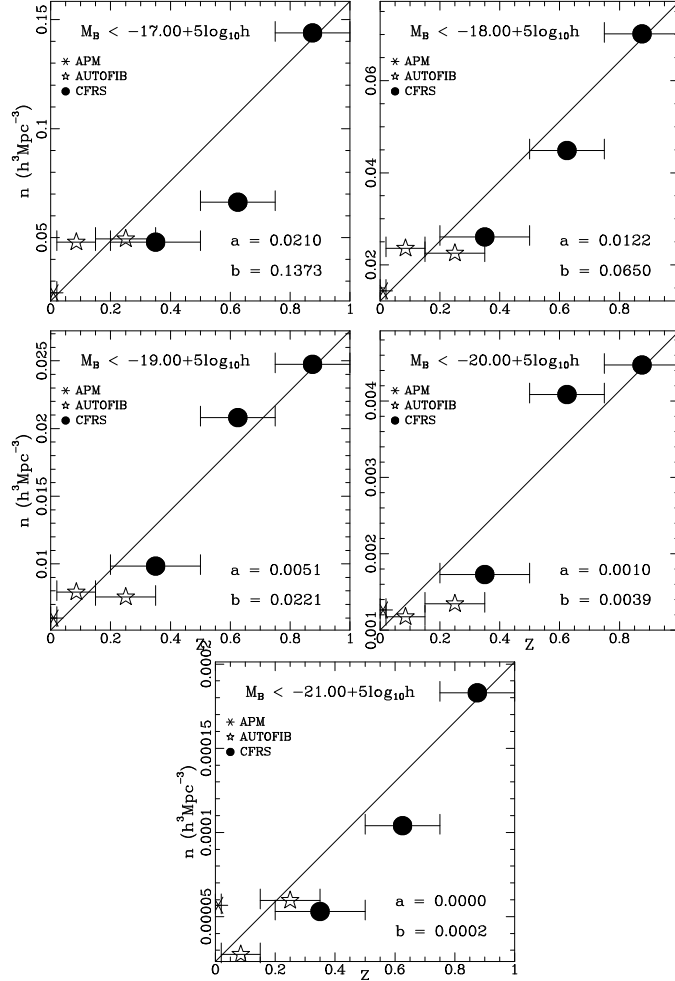


Fig. 2.— Spatial number density of galaxies with M_B (rest-frame) brighter than $-17 (+5\log_{10}h)$, -18 , -19 , -20 , and -21 absolute magnitude, as function of redshift. All points are obtained by integrating over the Schechter luminosity function with appropriate parameters as quoted by the different authors. The diagonals are linear approximations (not fits) to the functions, and their parameters are displayed ($n(z) = a + bz$).

function $S_{\text{SN}} = 0.0136 + 0.0670z$ ($100 \text{ yr}^{-1} (h^{-1}\text{Mpc})^{-3}$); the straight line in fig. 3 describes this curve. This line is not a least-square fit, for reasons mentioned earlier. We anchored the line at the $z = 0$ value since the Schechter function parameters are best determined in the local universe. It seems that a quadratic curve will fit the estimated data better; however, extrapolation of such a curve would not be a conservative choice for $z > 1$. Moreover, fig. 2 suggests a linear behavior of $n(z)$, the most important quantity that governs eq. 3-1. These considerations lead us to choose the linear approximation for $S_{\text{SN}}(z)$ as it appears in the plot.

In order to get the expression for the expected rate of SNe behind a lens with a $j\sigma$ magnitude–

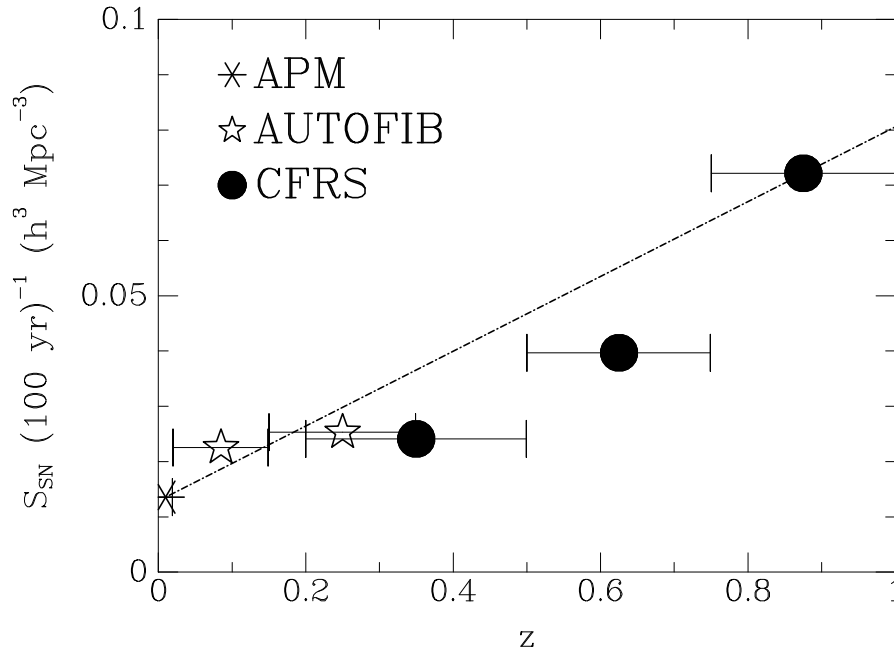


Fig. 3.— The calculated rate of SN per century per unit of comoving volume as function of redshift (eq. 3-1). The specific rate is taken to be $\mathcal{S}_{\text{SN}}(z = 0.4) = 0.82h^2 \text{ SNU}$. Symbols, Schechter luminosity function parameters, and redshift bins are identical to those used in fig. 2. The straight line is our underestimating model (not a fit, see text) for the rate evolution.

distance mismatch, we use the cross section and magnification probability (eqs. 2-2–2-3). The minimal magnification needed in order to establish the luminosity–distance discrepancy is A_{min} . For a $j\sigma$ discrepancy, $A_{\text{min}} = 10^{0.4j\Delta m}$. The expected rate is given by

$$\begin{aligned} \mathcal{R} &= \frac{1}{100} \int_{z_L}^{\infty} dz \frac{dR(z)}{dz} R^2(z) \frac{S_{\text{SN}}(z)}{(1+z)} \sigma_{\text{sis}}(A_{\text{min}}) \int_{A_{\text{min}}}^{\infty} dA P(A) \\ &\times \int_{-\infty}^{\infty} dM_{\text{SN}} P(M_{\text{SN}}) \Theta \left[m_{\text{lim}} - (M_{\text{SN}} + \Delta M_{\text{th}} + \mu(d_S^l) - 2.5 \log_{10}(A)) \right] \text{ yr}^{-1}, \quad (3-2) \end{aligned}$$

with the radial component of a comoving volume element ($R^2 dR = (d^M)^2 / (1 + \Omega_k H_0^2 (d^M)^2)^{1/2} d(d^M)$ cf. Carroll, Press, & Turner (1992) where $d^M(z)$ is the proper motion distance.) $\mu(d_S^l)$ is the distance modulus as a function of the luminosity distance. We take the survey magnitude limit for SN identification (as opposed to the follow-up) to be m_{lim} . Θ is the Heaviside step function that imposes the magnitude threshold for the detection of a SN. The threshold detection magnitude is expressed by ΔM_{th} , *i.e.* the difference between the peak magnitude and the identification magnitude we require. The factor $(1+z)^{-1}$ accounts for the cosmological time dilation. As mentioned above, we neglect a possible fainter image in our calculation.

A few comments have to be made regarding expression 3-2. To begin with, we have neglected the redshift dependence of \mathcal{S}_{SN} (which propagates to S_{SN}), albeit we use a relatively low redshift ($z = 0.4$) for it. This is in spite of the expected (and observed) increase of the specific rate with redshift. Even a mild increase reflects strongly in the expected rate. Another comment on

expression (3-2) regards the K-correction. Strictly speaking, since we integrated over $P(M)$ for rest-frame blue magnitude, a K-correction will shift SNe into a different observed band for each redshift, and thus also to different apparent magnitude (because of different zero points for different magnitudes). We did not include the K-correction for three reasons:

1. The K-correction for SNe of redshift higher than $z = 0.5$ has not yet been calculated (Kim, Goobar, & Perlmutter 1996).
2. The K-correction at $z \simeq 1$ generally translates an apparent magnitude limit in B (say 26) to be smaller in R and I (say 25–25.5). The signal-to-noise in R or I, though, decreases as well and therefore requires longer integration time.
3. As Goobar & Perlmutter (1995) pointed out, when one goes to higher redshift, the optimal filter is selected accordingly. Perlmutter *et al.* (1995) suggest that a more robust procedure (than K-correction) is to compare the LC in the band equivalent to the rest-frame B band.

In general, thus, all the apparent B magnitude limits we quote are higher than the required magnitude limits if observations are carried out in the appropriate bands (but recall that the signal-to-noise decreases in R and I).

We model the absolute magnitude distribution of the SNe Ia ($P(M_{\text{SN}})$ of eq. (3-2)) as a δ -function in peak absolute magnitude. As can be seen from figure 1a, the observed distribution is narrow, and slightly skewed. There is higher probability to find brighter-than-average absolute magnitudes than dimmer-than-average. By using a δ -function at the average, $P(M_{\text{SN}}) = \delta(\langle M_{\text{SN}} \rangle - M_{\text{SN}})$, we underestimate the observed rate predicted by eq. (3-2).

Choosing this distribution of M_{SN} simplifies eq. (3-2) to

$$\mathcal{R} = \frac{1}{100} \int_{z_L}^{\infty} dz \frac{dR(z)}{dz} R^2(z) \frac{S_{\text{SN}}(z)}{(1+z)} \times \min[\sigma_{\text{SIS}}(A'), \sigma_{\text{SIS}}(A_{\text{min}})] , \quad (3-3)$$

with

$$A' = \text{dex} \left[0.4 \left(\langle M_{\text{SN}} \rangle + \Delta M_{\text{th}} + \mu(d_S^l) - m_{\text{lim}} \right) \right] . \quad (3-4)$$

Already being equipped with S_{SN} , the SN rate in unit volume as a function of redshift (eq. 3-1), we calculate expression (3-3) in order to find the expected rate of observed SNe with luminosity–distance mismatch behind a cluster. We choose the cosmological parameters ($\Omega_m = 1$, $\Omega_\Lambda = 0$, $h = 1$). We require a typical SN to be found about 5 (rest-frame) days prior to peak luminosity. This is equivalent to $\Delta M_{\text{th}} \equiv \Delta M_{-5} = |M_{\text{SN}} - M_{\text{SN}-5}|$ of $\sim 0.1 - 0.3$ magnitudes. We assume a natural scatter in the LCS-luminosity relation of $\Delta m \equiv \Delta M_{\text{SN}} = 0.12$ (RPK2), and decide how many ΔM_{SN} away from the average relation we would like a SN to be detected in order to claim a mismatch. This value for Δm may be too optimistic for existing LCS methods. In principle, however, it is achievable especially if outlier SN are easily identified and eliminated.

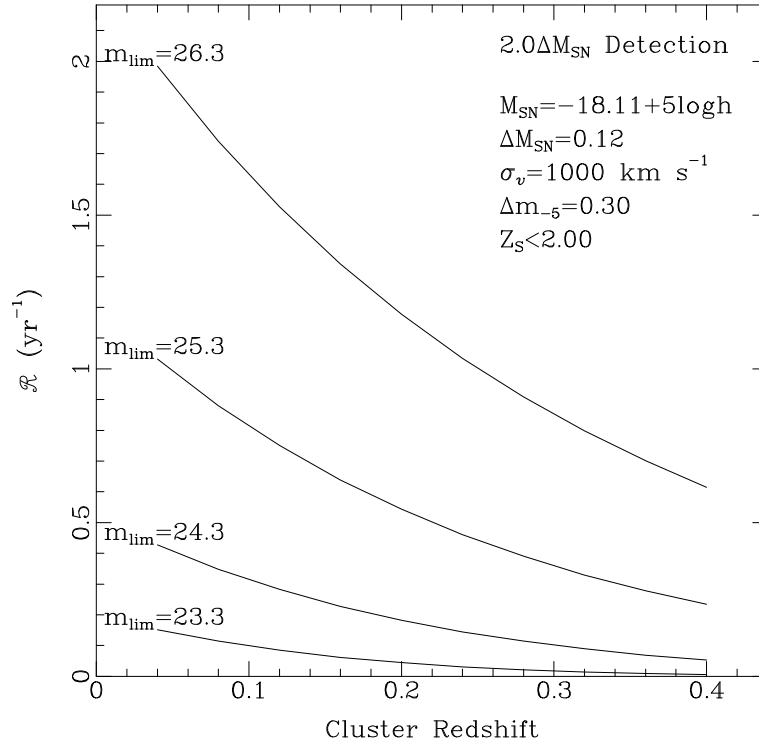


Fig. 4.— The expected detection rate of SNe Ia in the background of a lensing cluster as function of the lens redshift. The imposed requirement is that the mismatch between the LCS-corrected peak luminosity and the distance be twice the scatter of the former.

Figure 4 shows the expected rate for *detectable* SNe behind a cluster at different redshifts. We choose $\sigma_v = 1000 \text{ km s}^{-1}$ for the cluster velocity dispersion. The different curves correspond to different magnitude limits for the SN detection. Recall that these limits are a direct translation from the rest-frame B band to the actual observed bands, where one expects the limit to be $\sim 1-1.5$ magnitudes lower (because of the zero-point shift). The integration over z is carried out only up to $z = 2$ to achieve agreement with the observed surface number density, and in order not to extrapolate the redshift dependence of the galaxy number density too far. Since we did not include K-correction in our calculation, we do not specify the band of the magnitude limit. As was pointed out by Goobar & Perlmutter (1995), it is probably the I filter that is most suitable for $z \simeq 1$ SN detection and the I,J filters for SNe of $1 < z < 2$. Increasing the magnitude limit beyond 26.3 does not yield a higher rate because of the cutoff in the source redshift. The rate drops monotonically with lens redshift because the Einstein angle of a SIS is almost independent of lens redshift as long as $z_S \gg z_L$. The redshift dependence of the rate is thus determined by the volume behind the lens that is spanned by the almost constant angular cross section of the cluster.

Figure 4 indicates that if all LMC-like galaxies ($M_B < -17$ for $h = 0.57$) host SNe with the same average specific rate as observed at $z = 0.4$ (the contribution of galaxies dimmer than -17 to S_{SN} is small), then we can expect to observe 1-2 SNe behind each nearby cluster each year. Since

most SNe will be at higher redshift, the cosmic time dilation reduces the expected rate (*cf.* eqs. 3-2, 3-3) but at the same time widens the time window to catch the SN while its LC is rising. The necessary duration for the SN identification survey is therefore *not* inversely proportional to the ratio between the local and high- z expected rate.

3.3. The degeneracy removal

If a mismatch of Δm is found for a background SN, one has to decide what is the permitted range of variation for the SN absolute magnitude (recall the magnitude probability is asymmetric, *cf.* fig. 1a). For a permitted range of $k\sigma$, and a $j\sigma$ mismatch detection, the lower and upper limits for the magnification are $\text{dex}[0.4(j - k)\Delta M_{\text{SN}}] \leq A \leq \text{dex}[0.4(j + k)\Delta M_{\text{SN}}]$. These limits can immediately be translated to limits on the cluster velocity dispersion,

$$[\text{dex}[0.4(j - k)\Delta M_{\text{SN}}] - 1] \frac{\theta}{C} \leq \sigma_v^2 \leq [\text{dex}[0.4(j + k)\Delta M_{\text{SN}}] - 1] \frac{\theta}{C} \quad (3-5)$$

with $C = \theta_E/\sigma_v^2$. The significance of these limits is much increased when combined with other reconstruction methods (*e.g.* Kaiser & Squires 1993; Squires & Kaiser 1996; Schneider & Seitz 1995; Seitz & Schneider 1995, 1996, 1997; Bartelmann *et al.* 1996).

Being a point source, the SN probes a single line-of-sight that intersects the cluster. Inferring limits on the cluster mass from limits on A may bear two caveats; if the SN line-of-sight happens to pass near a cluster galaxy, the galaxy adds to the magnification, and the simple interpretation of the limits on A in terms of limits on the cluster mass is no longer valid. Barring dramatic magnification bias, the two-dimensional filling factor of galactic critical curves beyond θ_E is very small, and therefore the galaxy contributions can generally be ignored.

A similar contribution to the magnification may arise due to intervening low mass objects (intracluster MACHOs). We discuss this possibility in the next section.

4. Intracluster Machos

The requirement for high enough a magnification in order to identify a mismatch in the luminosity-distance relation is essential only if we like to remove the mass sheet degeneracy. However, even if a SN is observed at radii larger than $\theta_{\text{max}}(A_{\text{min}})$, it is still very useful as a point-like probe for the dense environment of the cluster. The spectral line identification, and the family of LCSs, allow for an identification of many possible modulations of the light curve. The main source for such modulations are compact objects in the intracluster medium which induce microlensing events on top of the cluster magnification.

The Einstein radius of a point mass M is

$$r_E = \left(\frac{4GM}{c^2} D_{\text{eff}} \right)^{1/2}. \quad (4-1)$$

$D_{\text{eff}} = D_L D_{LS} D_S^{-1}$ is the effective lensing distance, with $D_{L,S,LS}$ the angular diameter distance to the lens, the source, and between lens and source, respectively. Inserting numbers,

$$r_E = 4.3 \times 10^{16} \text{ cm} \left(\frac{M}{M_\odot} \right)^{1/2} \left(\frac{D_{\text{eff}}}{\text{Gpc}} \right)^{1/2}. \quad (4-2)$$

The time scale for a source crossing the Einstein disk is

$$\Delta t_{\mu L} = \frac{2r_E}{v_{\text{eff}}} = 27.3 \text{ yr} \left(\frac{M}{M_\odot} \right)^{1/2} \left(\frac{D_{\text{eff}}}{\text{Gpc}} \right)^{1/2} \left(\frac{v_{\text{eff}}}{10^3 \text{ km s}^{-1}} \right)^{-1}, \quad (4-3)$$

with the effective relative velocity $v_{\text{eff}} \simeq \sqrt{2}\sigma_v$ of microlens and source. The time scale Δt_{SN} of a SN Ia at redshift $z_s \sim 1$ is of order 100 days. Even for higher redshifts, this is the maximum relevant time-scale (half a year) due to observational constraints. The microlensing time scale $\Delta t_{\mu L}$ is therefore compatible with Δt_{SN} only for very small microlens masses, $M \sim 10^{-4} M_\odot$.

The time scale may be shorter due to the expansion of the SN photosphere. An estimate for this limit is obtained by requiring that the angular size of the SN not exceed that of the Einstein radius. For a rest-frame expansion rate of $v_{\text{SN}} \simeq 10^9 \text{ cm s}^{-1}$, the angular size of the SN photosphere at *observed* time t is $\theta_{\text{SN}} = v_{\text{SN}} t (1 + z_S)^{-1} D_S^{-1}$. This angular size should be compared to $r_E D_L^{-1}$ to give

$$\Delta t_{\text{lim}} = \frac{r_E (1 + z_S)}{v_{\text{SN}}} \frac{D_S}{D_L}. \quad (4-4)$$

For $D_S D_L^{-1} \simeq 10$, $M \sim 10^{-4} M_\odot$, and $z_S = 1 - 2$, Δt_{lim} amounts to ~ 30 days. For smaller masses, or later observational times, a microlensing event may still be detected, but the typical microlensing amplification is suppressed, and eventually disappears (*cf.* Schneider & Wagoner 1987). The SN time scale is thus $\Delta t_{\text{SN}} = \min(100 \text{ d}, \Delta t_{\text{lim}})$.

4.1. Point mass in a cluster

An isolated point mass embedded in a SIS cluster is the typical case of a Chang-Refsdal lens (Chang & Refsdal 1979). Shear and convergence of the cluster at the position of the microlens increase the cross section of the microlens, which we here define to be the area enclosed by the critical curve of the microlens. While the cross section (in units of an area rather than a solid angle) of an isolated microlens is $\tilde{\sigma}_0 = \pi r_E^2$, the corresponding cross section of the Chang-Refsdal lens is $\tilde{\sigma}_{\text{C-R}}(\theta) \simeq A(\theta) \tilde{\sigma}_0$, to excellent accuracy. $A(\theta)$ is the magnification of the cluster at the position θ of the microlens, *cf.* eq. (2-1).

Let $n(\theta)$ be the surface number density of microlenses at radius θ in the cluster. We assume that $n(\theta)$ is a fixed fraction f of the cluster’s surface mass density $\Sigma(\theta)$,

$$n(\theta) = \frac{f \Sigma(\theta)}{M} = \frac{f \Sigma_{\text{cr}} \theta_{\text{E}}}{2\theta M}, \quad (4-5)$$

where we have used the critical surface mass density

$$\Sigma_{\text{cr}} = \frac{c^2}{4\pi G} D_{\text{eff}}^{-1} \quad (4-6)$$

and the (angular) Einstein radius of the cluster (eq. (2-1)). The average number of microlenses straddled by a macroimage at position θ is

$$N(\theta) = n(\theta) \tilde{\sigma}_{\text{C-R}}(\theta). \quad (4-7)$$

Inserting $\tilde{\sigma}(\theta) = A(\theta)\pi r_{\text{E}}^2$, and using eqs. (4-1) and (4-6), eq. (4-7) becomes

$$N(\theta) = \frac{f A(\theta) \theta_{\text{E}}}{2\theta}. \quad (4-8)$$

This is the equivalent to the microlensing “optical depth” at angular distance θ from the cluster center. In order to find the average number of microlenses straddled by *any* macroimage, we need to average $N(\theta)$ with the probability distribution for image positions, $P(\theta)$. Assuming the sources are randomly distributed in the source plane, we can write (*cf.* eq. (2-3))

$$P(\theta)d\theta = (A_{\text{min}} - 1)^2 \frac{2(\theta - \theta_{\text{E}})}{\theta_{\text{E}}^2} d\theta. \quad (4-9)$$

This probability function is still not the probability of observing a SN at angle θ . The latter is given by the additional magnitude limit imposed by the observations. For this we need not find a SN with a luminosity-distance mismatch, but merely a SN that exceeds the magnitude threshold for identification. The rate of observed SNe is given by a similar expression to eqs. (3-2, 3-3). We again assume a δ -function for the SN absolute magnitude distribution, and eliminating the mismatch constraint we require arbitrarily $A_{\text{min}} = 1.1$. This value is still within the scale where it is adequate to use the SIS model for the cluster density profile. Figure 5 shows the expected detection rate for SN Ia with the rest of the parameters identical to those of fig. 4. If $m_{\text{lim}} \geq 26.3$ all ~ 10 expected SN behind nearby clusters can be used for the macho detection, though only a small fraction of them ($\sim 1 : 5$) are suitable for a mismatch detection.

We do not know *a priori* where an individual SN will show up in the cluster background. Based on the probability function (4-9) we can however predict the average optical depth. Combining eqs. (4-8) and (4-9), we find

$$\langle N \rangle = \int_{\theta_{\text{E}}}^{\theta_{\text{max}}} d\theta P(\theta) N(\theta) = f (A_{\text{min}} - 1). \quad (4-10)$$

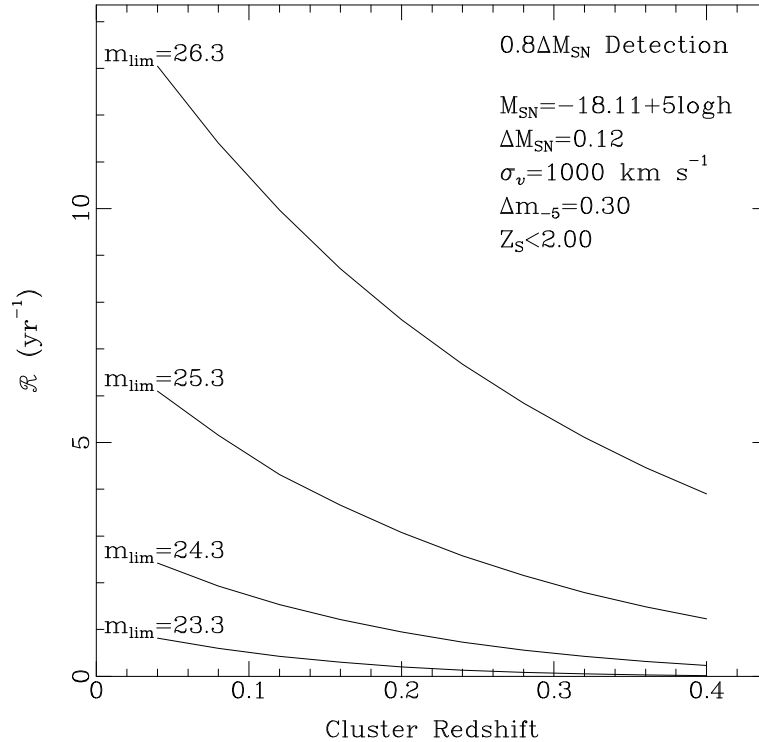


Fig. 5.— The expected detection rate of SNe Ia in the background of a lensing cluster as function of the lens redshift. Minimal magnification of $A_{\text{min}} = 1.1$ is assumed corresponding to $\theta \simeq 3.5 - 4.5$ arcmin. in the plotted range.

Note that $\langle N \rangle$ does not depend on the mass of the individual microlenses. The probability for a microlensing event is therefore independent of the microlens mass, but the microlensing time scale selects for masses of order $10^{-7} - 10^{-4} M_{\odot}$.

In order to estimate the total number per year of microlensing events that we expect for a given cluster, the probability to observe a SN should be folded in. The rate is then given by (cf. eq. 3-3)

$$\mathcal{R}_{\mu\text{L}} \simeq \frac{f(A_{\text{min}} - 1)}{100} \int_{z_L}^{\infty} dz \frac{dR(z)}{dz} R^2(z) \frac{S_{\text{SN}}(z)}{(1+z)} \frac{\Delta t_{\text{SN}}(z)}{\Delta t_{\mu\text{L}}(z)} \times \min[\sigma_{\text{sis}}(A'), \sigma_{\text{sis}}(A_{\text{min}})] \text{ yr}^{-1}. \quad (4-11)$$

Figure 6 shows the expected number of microlensing events behind clusters of various redshifts. We assumed $f = 0.01$ and $\sigma_v = 1000 \text{ km s}^{-1}$. The magnitude limit for the SN identification is assumed to be 26.3 (see 3.2), and $A_{\text{min}} = 1.09$ which corresponds to $\theta \simeq 3.5 - 4.5$ arcmin. in the plotted redshift range. This rate is relevant for the MACHO mass range $(10^{-4} - 10^{-7})M_{\odot}$.

If a microlensing event leaves its signature on the LCS, what would this signature look like? Figure 7 shows examples of three SN Ia LC's, modified by microlensing due to $10^{-4}M_{\odot}$ intracluster MACHOs. We modeled the LCS by $-M(d) = (a \exp[-(d/\sigma_d)^2] + s) \times [1 + b(d/d_t)]$ with d in days, and the parameters $a = 3$, $\sigma_d = 20$, $s = 17.2$, $b = -1/63$, and $d_t = 50$. This functional

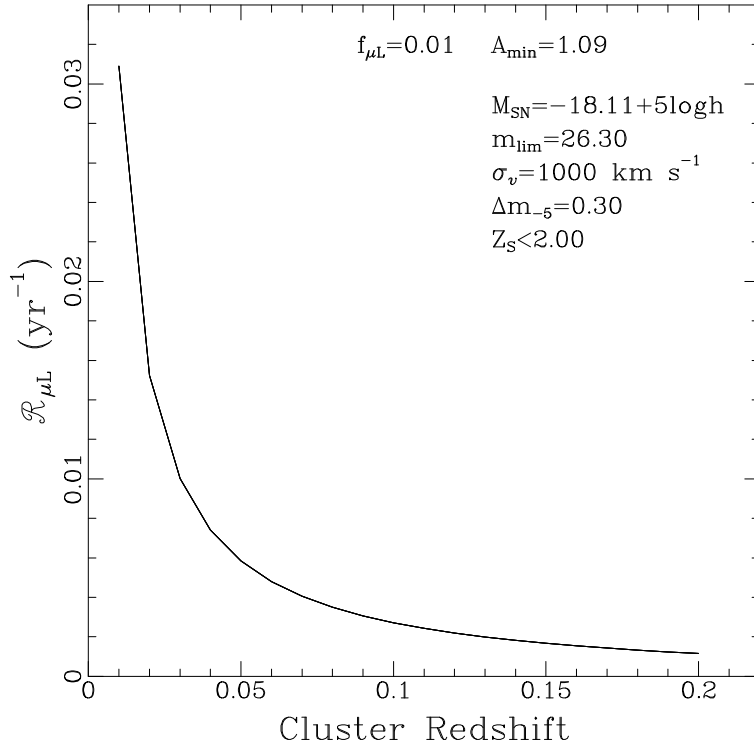


Fig. 6.— The expected detection rate of microlensing events in the background of a lensing cluster as a function of the lens redshift. We assumed $f = 0.01$, $\sigma_v = 1000 \text{ km s}^{-1}$, and Δt_{SN} as dictated by the SN expansion rate (Δt_{lim} , Eq. 4-4). The magnitude limit for the SN identification is assumed to be 26.3 (see 3.2), and $A_{\text{min}} = 1.09$. The relevant MACHO mass range is $(10^{-4} - 10^{-7}) M_{\odot}$.

form, and the parameters, provide a curve very similar to the template RPK2 used for SN 91T [$d \in (-10, 150)$ days]. For the microlensing events, we use $z_L = 0.2$, $z_S = 0.8$, and $\sigma_v = 10^3 \text{ km s}^{-1}$ for the SIS cluster profile. We assume a SN angular size smaller than the MACHO Einstein radius throughout the event duration. The lower right panel of the figure depicts the caustic curve of the microlens projected onto the source sphere and the tracks of the SN relative to the microlens. The figure nicely demonstrates that it should not be too hard a task to separate the microlensing event signature from the LCS of the SN. The LCSs of the SNe are differently modeled in different bands. The microlensing event on the other hand appears identical in all bands thanks to its achromatism. This dichotomy in nature makes the deconvolution of the two easy to accomplish.

5. Summary and Conclusions

We have proposed to look for SN type Ia behind nearby rich clusters. The expected rate of detectable SN behind such clusters is of the order of 10 SN yr^{-1} per cluster, about 20% of which can be used alone as tools to remove the mass sheet degeneracy. The rest of the detected SN can

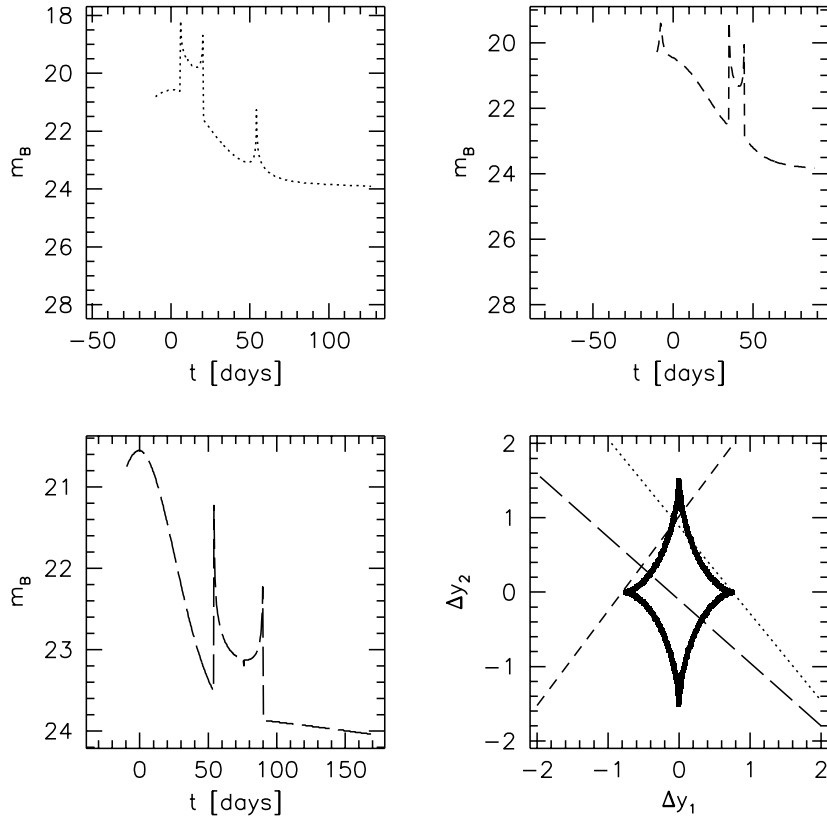


Fig. 7.— Examples for three microlensed SN Ia light curves. The SNe Ia are assumed at redshift $z_S = 0.8$, the cluster at redshift $z_L = 0.2$. The source tracks relative to the microlens are chosen randomly. The microlens mass is $M = 10^{-4} M_\odot$, and the effective relative velocity is $v_{\text{eff}} = \sqrt{2} 10^3 \text{ km s}^{-1}$. The cluster magnification at the position of the microlens was chosen to be 4. $\Delta y_{1,2}$ are in units of r_E , projected on the source sphere. The lower right panel depicts the caustic curve of the microlens and the tracks of the SN relative to the microlens.

be combined together for the same purpose. Since the magnification scales like θ^{-1} and the number of sources scales like $\sim \theta^2$ (neglecting magnification bias), we expect the signal-to-noise ratio to be constant. Statistical use of the SNe on large radii yields a similar signal-to-noise ratio as for the SNe that exceeded the mismatch threshold.

Any of the detected SN can serve as a point source with a typical light curve shape. Any modulation of this light curve shape, or lack thereof, can put limits on the mass fraction of the cluster in the form of $10^{-7} < M/M_\odot < 10^{-4}$ MACHOs.

This proposed survey shifts the focus from high redshift clusters as targets for high redshift SNe to low redshift clusters as foreground lenses for the same, and farther SNe. At the same time, the nearby observed cluster enhances the probability of finding serendipitous SNe in it. The use of the cluster SNe as point sources for MACHO search is somewhat less efficient because of the

relatively small effective lensing distance D_{eff} , and the unknown position of the source within the cluster. The monitoring procedure of current observations will have to be modified, namely to allow for longer gaps between successive observations of the same cluster, but more observations in total during the year. The proposal demands a higher magnitude limit than the values that are currently used, both for the identification and for the follow-up. These limits, however, are not out of reach.

Let us list again all the choices we have made to result in an underestimate of the mismatch SNe rate.

1. We do not take into account the fainter image when multiple images appear on the image plane.
2. We took the specific SN Ia rate at $z = 0.4$ and used it as the representative value for higher redshifts despite the prediction of increasing rate with redshift.
3. We choose a δ -function to represent the probability distribution of the SN absolute blue magnitude. The δ -function is centered on the mean, even though the median of the distribution seems to be on the bright side. On the other hand, note we have ignored a possible Malmquist bias in the Hamuy *et al.* (1996a) sample, a bias that tends to slightly shift the average towards brighter magnitudes.
4. We considered only SNe that exceed the detection (magnitude limit) threshold 5 days (rest-frame) prior to peak luminosity. A weaker requirement (*i.e.* only 0.2 magnitudes below peak) may suffice if a denser time sampling is devised, or if the SN is intrinsically more luminous than average (and therefore rises and declines more slowly).
5. We require a mismatch of twice the natural scatter in the LCS-luminosity relationship. A more modest requirement may be sufficient to establish limits on the surface mass density along the line-of-sight.
6. We only integrate in redshift up to $z = 2$ because of lack of knowledge of the number density of galaxies beyond this range. Note that if we are not willing to extrapolate the galaxy number density beyond $z \simeq 1.5$, but we still like to satisfy the observed surface number density of galaxies, the number density should rise even more steeply than assumed beyond $z = 1$. If this is the case, more SN Ia fall under the magnitude limit of the survey, and the rate increases correspondingly.

It seems that the main challenge for this proposed method is the high accuracy photometry needed. Two groups are currently conducting a hunt for high redshift SNe (the SN cosmology project based at Lawrence Berkeley National Laboratory (Perlmutter *et al.* 1997); the high- z SN search team based in Mt. Stromlo, Australia (Schmidt *et al.* 1996)). One survey fits this paper

proposal if higher magnitude limits are applied (Abell cluster SN search, University of Washington). These surveys' objective is generally quite different from the investigation of galaxy clusters (nevertheless, we have just heard that the SN cosmology project intend to propose a survey in the spirit of this paper). The expertise they have acquired for determining the value of the cosmological background parameters should serve them well in pursuing the nature and distribution of matter within this background.

We thank Saul Perlmutter for helpful comments on the manuscript. This work was supported in part by the NASA ATP grant (NAG 5-3061) (TK) and by the Sonderforschungsbereich 375 of the Deutsche Forschungsgemeinschaft (MB).

REFERENCES

- Bartelmann, M. & Narayan, R. 1995, *ApJ*, 451, 60
- Bartelmann, M., Narayan, R., Seitz, S., & Schneider, P. 1996, *ApJ*, 464, 115
- Bertschinger, E. 1985, *ApJS*, 58, 39
- Branch, D. & Tammann, G.A. 1992 *ARA&A*, 30, 359
- Branch, D. & Miller, D.L. 1993, *ApJ*, 405, L5
- Branch, D., Romanishin, W., & Baron, E. 1996, *ApJ*, 465, 73
- Broadhurst, T., Taylor, A., Peacock, J. 1995, *ApJ*, 438, 49
- Cappellaro, E., Turatto, M., Benetti, S., Tsvetkov, D.Yu., Bartunov, O.S., & Makarova, I.N. 1993a, *A&A*, 268, 472
- Cappellaro, E., Turatto, M., Benetti, S., Tsvetkov, D.Yu., Bartunov, O.S., & Makarova, I.N. 1993b, *A&A*, 273, 838
- Cappellaro, E., Turatto, M., Tsvetkov, D.Yu., Bartunov, O.S., Pollas, C., Evans, R., & Hamuy, M. 1997, *AJ*, 322, 431
- Carroll, S.M., Press, W.H., & Turner, E.L., 1992, *ARA&A*, 30, 499
- Chang K., Refsdal S. 1979, *Nature*, 282, 561
- Ellis, R.S., Colless, M., Broadhurst, T., Heyl, J., & Glazebrook, K. 1996, *MNRAS*, 280, 235
- Falco, E.E., Gorenstein, M.V., Shapiro, I.I. 1985, *ApJ*, 289, L1
- Filmore, J.A., & Goldreich, P. 1984, *ApJ*, 281, 1
- Frieman, J.A. 1996, preprint, astro-ph/9608068.
- Goobar, A. & Perlmutter, S. 1995, *ApJ*, 450, 14
- Gunn J., & Gott J.R. 1972, *ApJ*, 176, 1

- Hamuy, M., Phillips, M.M., Maza, J., Suntzeff, N.B., Schommer, R.A., & Avileś, R. 1995, AJ, 109, 1
- Hamuy, M., Phillips, M.M., Schommer, R.A., Suntzeff, N.B., Maza, J., & Avileś, R. 1996a, AJ, 112, 2391
- Hamuy, M. *et al.* 1996b, AJ, 112, 2408
- Hoffman, Y. 1988, ApJ, 328, 489
- Kaiser, N. 1995, ApJ, 439, L1
- Kaiser, N., Squires, G. 1993, ApJ, 404, 441
- Kim, A., Goodbar, A., & Perlmutter, S. 1996, PASP, 108, 190
- Kneib, J.-P., Ellis, R.S., Smail, I., Couch, W.T., Sharples, R.M. 1995, ApJ471, 643
- Kovner, I. & Paczyński, B. 1988, ApJ, 335, L9
- Lilly, S.J., Cowie, L.L., & Gardner, J.P. 1991, ApJ, 369, 79
- Lilly, S.J., Tresse, L., Hammer, F., Campton, D., & Le Fèvre, O. 1995 ApJ, 455, 108
- Loveday, J., Peterson, B.A., Efxathiou, G., Maddox, S.J., 1992, ApJ, 390, 338
- Metcalfe, N., Shanks, T., Fong, R., & Jones, L.R. 1991, MNRAS, 249, 498
- Metcalfe, N., Shanks, T., Fong, R., & Roche, N. 1995, MNRAS, 273, 257
- Muller, R.A., Marvin, H.J., Pennypacker, C.R., Perlmutter, S., Sasseen, T.P., & Smith, C.K. 1992, ApJ, 384, L9
- Navarro, J.F., Frenk, C.S., White, S.D.M., 1996, ApJ, 462, 563
- Pain, R. *et al.* 1995, ApJ, 473, 356
- Perlmutter, S. *et al.* 1995, ApJ, 440, L41
- Perlmutter, S. *et al.* 1997, ApJ, 483, 565
- Phillips, M. 1993, ApJ, 413, L105
- Riess, A.G., Press, W.H., Kirshner, R.P. 1995, ApJ, 438, L17
- Riess, A.G., Press, W.H., Kirshner, R.P. 1996, ApJ, 473, 88
- Schmidt, B.P. *et al.* 1996, Bull. Am. Ast. Soc., 189, 108.05
- Schneider, P. & Wagoner, R.V. 1987, ApJ, 314, 154
- Schneider, P. & Seitz, C., 1995, A&A, 294, 411
- Seitz, C. & Schneider, P. 1995, A&A, 297, 287
- Seitz, C. & Schneider, P. 1996, A&A, 305, 383
- Seitz, C. & Schneider, P. 1997, A&A, 318, 687
- Smail, I., Hogg, D.W., Yan, L., & Cohen, J.G. 1995 ApJ, 449, L105

- Soucail, G. & Fort, B. 1990, *A&A*, 243, 23
- Squires, G. & Kaiser, N. 1996, *ApJ*, 473, 65
- Turatto, M., Cappellaro, E., & Benetti, S. 1994, *AJ*, 108, 202
- Tyson, J.A. 1988, *AJ*, 96, 1
- Tyson, J.A. & Fischer, P. 1995, *ApJ*, 446, L55
- van den Bergh, S. & McClure, R.D., 1994, *ApJ*, 425, 205
- Vaughan, T.E., Branch, D., Miller, D.L., & Perlmutter, S. 1995, *ApJ*, 439, 558
- Wambsganss, J., Cen, R., Xu, G., Ostriker, J.P. 1997, *ApJ*, 475, L81